

Highly-Ionized Oxygen Absorbers in the Intergalactic Medium

S. R. Furlanetto,^{*} L. A. Phillips, and M. Kamionkowski

California Institute of Technology, Mail Code 130-33, Pasadena, CA 91125, USA

17 September 2018

ABSTRACT

Recent ultraviolet and X-ray observations of intergalactic OVI and OVII absorption systems along lines of sight to bright quasars have opened a new window onto the “warm-hot intergalactic medium” (WHIM). These systems appear to provide a significant reservoir for baryons in the local universe, and comparison to cosmological simulations suggests that their abundance roughly matches theoretical predictions. Here we use analytic arguments to elucidate the physical properties of the absorbers and their role in structure formation. We first show that if the absorbers result from structure-formation shocks, the observed column densities naturally follow from postshock-cooling models, if we include fast-cooling shocks as well as those that cannot cool within a Hubble time. In this case, the known OVI absorbers should show stronger OVII absorption than expected from collisional-ionization equilibrium (and much more than expected for photoionized systems). We then argue that higher-temperature shocks will be spatially associated with more massive virialized objects even well outside the virial radius. Thus the different oxygen ions will trace different structures; OVII absorbers are the most common because that ion dominates over a wide temperature range (corresponding to a large range in halo mass). If each dark-matter halo is surrounded by a network of shocks with total cross section a few times the size of the virialized systems, then we can reproduce the observed number densities of absorbers with plausible parameters. A simple comparison with simulations shows that these assumptions are reasonable, although the actual distribution of shocked gas is too complex for analytic models to describe fully. Our models suggest that these absorbers cannot be explained as a single-temperature phase.

Key words: intergalactic medium – quasars: absorption lines

1 INTRODUCTION

The cosmic-web paradigm has had a great deal of success in explaining the distribution of matter in the intergalactic medium (IGM) at moderate redshifts $z \sim 3$, especially in the Ly α forest (e.g., Rauch 1998). In this picture, dark matter collapses through gravitational instability into sheets and filaments before accreting onto bound structures such as galaxies, groups, and clusters (which appear at the intersections of filaments). The baryons also accrete onto these structures, but (in addition to gravitational forces) they are subject to fluid effects such as shock heating. At $z \sim 3$, the infall velocities are modest relative to the ambient sound speed and shocks are relatively unimportant except in collapsed objects. However, at the present day, shocks have heated most of the filamentary gas to $T \gtrsim 10^5$ K (Cen & Ostriker 1999); this gas is now known as the “warm-hot IGM” (WHIM). Simulations predict that this phase contains a substantial fraction of the baryons (Cen & Ostriker 1999; Davé et al. 2001). The characteristic temperature $T \sim 10^6$ K corresponds to the postshock temperature that has collapsed over the nonlinear mass scale in one Hubble time.

Unfortunately, most of the WHIM lies at a modest density

(~ 10 –100 times the cosmic mean) and in a temperature regime with few observational signatures; the hydrogen column densities are small because of collisional ionization and the gas is not hot enough to emit substantial bremsstrahlung radiation. As such, the WHIM has thus far only been detected through absorption of highly-ionized metals (specifically OVI, OVII, and possibly OVIII). Space-based ultraviolet spectrographs (including STIS on the *Hubble Space Telescope* and the *Far Ultraviolet Spectroscopic Explorer*) have allowed relatively straightforward detections of the OVI $\lambda\lambda 1032, 1038$ doublet along lines of sight to nearby bright quasars (Tripp et al. 2000; Tripp & Savage 2000; Oegerle et al. 2000; Sembach et al. 2001; Savage et al. 2002; Shull et al. 2003; Richter et al. 2004; Prochaska et al. 2004; Tumlinson et al. 2005; Danforth & Shull 2005). The inferred number density of absorption systems is large ($dn/dz \sim 15$), suggesting that these systems constitute a significant baryon reservoir. However, in collisional-ionization equilibrium (CIE), OVI only exists near the lower end of the WHIM temperature range. According to the simulations, most of the gas can only be probed through OVII or OVIII absorption, both of which require X-ray studies. The current generation of instruments does not have the sensitivity to measure the weak absorption expected from the IGM, and there are relatively few firm detections. A number of groups have found OVII and

^{*} Email:sfurlane@tapir.caltech.edu

OVIII absorption at $z = 0$ that may be associated with the Local Group (Nicastro et al. 2002; Rasmussen et al. 2003; Fang et al. 2003). Nicastro et al. (2005) recently discovered two OVII absorbers along the line of sight to the blazar Mkn 421 during an outburst. Other detections have relatively low significance or lack confirmation from different instruments (e.g., Fang et al. 2002). Nevertheless, the Mkn 421 line of sight suggests an even higher number density than OVI ($dn/dz \sim 60$), albeit with large statistical uncertainties.

Comparison to lines of sight extracted from simulations suggests that these number densities are comparable to theoretical expectations (Hellsten et al. 1998; Cen et al. 2001; Fang & Bryan 2001; Fang et al. 2002; Chen et al. 2003). Detailed quantitative tests are difficult because of the large uncertainties on both the observational and theoretical sides (with the latter depending primarily on the unknown distribution of metals in the IGM), but the overall consistency is a reassuring confirmation of the cosmic-web paradigm. However, the existing studies have not addressed many questions about their physical origin or characteristic environment. As a result, we lack a clear picture of their specific role in the structure-formation process. For example, do they probe outlying filamentary gas, gas more closely associated with galaxies, or something entirely different? Do the OVI and OVII absorbers probe distinct environments, and do the two ions have different physical origins? What sets the observed column densities?

In this paper, we provide an analytic framework to answer these questions. This is clearly a difficult proposition: the WHIM is nonlinear and inherently asymmetric, so it is difficult to model analytically. Nevertheless, models describing the gross properties of the WHIM do exist (Nath & Silk 2001; Valageas et al. 2002; Furlanetto & Loeb 2004), and it is interesting to consider what these simple arguments reveal about the absorbers. Moreover, if shocks are ultimately responsible for heating gas to the WHIM temperatures, simple models of postshock cooling can help to explain the properties of the absorbers (Heckman et al. 2002). We will connect these two approaches in order to identify the key properties of the absorbers and how they may relate to collapsed objects.

The plan of this paper is as follows. In §2, we show how postshock cooling predicts characteristic column densities for the absorbers. We then construct a simple analytic model to predict the abundance of IGM oxygen absorbers in §3. We highlight some of the strengths and weaknesses of this model by comparing to cosmological simulations in §4. In §5, we show that comparing the OVI and OVII columns can robustly distinguish shock-heated and photoionized OVI absorbers. Finally, we conclude in §6.

We will primarily be concerned with OVI, OVII, and OVIII in this paper. For reference, we list details of their strongest transitions here. OVI has a UV doublet at $\lambda = 1032, 1038$ Å; the corresponding oscillator strengths are $f_{\text{osc}}^{\text{OVI}} = 0.133, 0.0660$. The most prominent OVII line is a He α transition with $\lambda = 21.602$ Å and $f_{\text{osc}}^{\text{OVII}} = 0.6945$, while that for OVIII is a Ly α transition with $\lambda = 18.97$ Å and $f_{\text{osc}}^{\text{OVIII}} = 0.416$. To avoid any assumptions about the velocity widths of each line, we will present all of our results in terms of column density N_{ion} . Observations are instead often presented in terms of equivalent width W (which is the fundamental observable). In the unsaturated limit, the two quantities are related (in cgs units) via $W = 8.85 \times 10^{-13} N_{\text{ion}} f_{\text{osc}} \lambda^2$ (e.g., Spitzer 1978). (For OVI, W is usually, though not universally, quoted for the stronger of the two doublet transitions.)

Throughout our discussion we assume a cosmology with $\Omega_m = 0.3$, $\Omega_\Lambda = 0.7$, $\Omega_b = 0.046$, $H_0 = 100h \text{ km s}^{-1} \text{ Mpc}^{-1}$

(with $h = 0.7$), $n = 1$, and $\sigma_8 = 0.9$, consistent with the most recent measurements (Spergel et al. 2003).

2 THE CHARACTERISTIC COLUMN DENSITIES

We will begin with the simple question of whether shock heating can account for the observed column densities of OVI absorbers. A number of recent observations have found a large number of such systems in the local universe, with typical column densities in the range $N_{\text{OVI}} \approx 2-20 \times 10^{13} \text{ cm}^{-2}$ (e.g., Tripp et al. 2000; Sembach et al. 2001; Richter et al. 2004; Prochaska et al. 2004). While the lower limit may be an observational selection effect (but see Danforth & Shull 2005), the rapid decline in abundance as the column density approaches 10^{14} cm^{-2} suggests that this is a characteristic maximum strength.

Heckman et al. (2002) provide a simple argument for why we should expect shocks to produce columns in this range. Consider a parcel of gas that is shocked to a temperature T_s . It will flow away from the shock with a velocity v_g (fixed by the jump conditions). After a time $t_{\text{cool}} = 3kT_s/n_s \Lambda$ it will have radiated its thermal energy and no longer be highly ionized; here n_s is the postshock gas density and Λ its normalized cooling rate in $\text{ergs cm}^3 \text{ s}^{-1}$. If we view the system along a plane perpendicular to the shock, and if the gas cools fully, we therefore expect to see highly-ionized gas along a path length $l_{\text{cool}} \approx v_g t_{\text{cool}}$ with a corresponding column density $N \approx n_s l_{\text{cool}}$. Thus

$$N_{\text{OVI}} = f_{\text{OVI}} Z [\text{O/H}]_{\odot} n_s v_g t_{\text{cool}} \quad (1)$$

where $[\text{O/H}]_{\odot} = 10^{-3.07}$ is the oxygen abundance by number in gas with solar metallicity (using the abundances of Sutherland & Dopita 1993), Z is the metallicity in solar units, and f_{OVI} is the fraction of oxygen atoms in the fifth ionized state. We note that the postshock speed is directly related to the postshock temperature via

$$v_g = \left(\frac{kT_s}{3\mu m_p} \right)^{1/2} \approx 50 \left(\frac{T_s}{10^6 \text{ K}} \right)^{1/2} \text{ km s}^{-1}, \quad (2)$$

where we have assumed that the shock is strong (so that $v_g = v_s/4$, with v_s the speed of the shock) and μm_p is the mean molecular mass. Heckman et al. (2002) emphasized that for moderately enriched gas, $\Lambda \propto Z$ (e.g., Sutherland & Dopita 1993). In this fully-cooled case, we therefore expect the column density to be *independent* of the metallicity and physical density.

We note that there is some tentative observational evidence for such a picture. Shull et al. (2003) and Tumlinson et al. (2005) each found pairs of OVI absorbers displaced by $v_s \gtrsim 200 \text{ km s}^{-1}$ from associated HI and/or low-ionization state metal absorbers. They suggested that the velocity difference may be characteristic of a shock.

Of course, equation (1) is only approximate because both t_{cool} and f_{OVI} depend on temperature. To properly compute the column density, we need to trace the (non-equilibrium) ionic abundances throughout the cooling (e.g., Dopita & Sutherland 1996). Fortunately, we can estimate the result reasonably well because f_{OVI} peaks sharply around a characteristic temperature, as we show in Figure 1a. We have computed the ionization fractions f_{ion} of the highly-ionized states of oxygen using Cloudy (version 94, Ferland 2001) for gas in CIE. We see that OVI is extremely sensitive to the gas temperature; $f_{\text{OVI}} \sim 0.3$ at $T \approx 10^{5.45} \text{ K}$ but drops steeply away from this value. The ionization fraction for OVII,

on the other hand, rises rapidly to $f_{\text{OVII}} \sim 1$ in the same temperature range for which OVI rises, but it remains large for all $10^{5.5} \text{ K} < T < 10^{6.5} \text{ K}$. This is a simple consequence of the lone $n = 2$ electron in OVI, which is much easier to strip than the $n = 1$ electrons in OVII: the ionization potentials of OVI and OVII are 138.1 and 739.3 eV, respectively. The plateau in f_{OVI} at $T \sim 10^6 \text{ K}$ and $f_{\text{OVI}} \sim 0.003$ occurs for the same reason. Clearly, OVI will come from gas in a narrow temperature range. Figure 1b shows the ratio of the cooling time to H_0^{-1} , also computed with Cloudy,¹ for a range of metallicities. In the plot we assume that $\Delta = 10$, where $\Delta = n/\bar{n}$ is the gas density relative to the cosmic mean; of course $t_{\text{cool}} \propto \Delta^{-1}$. The cooling time drops rapidly as we approach $T \sim 10^{5.45} \text{ K}$ from above (partly because of the strong OVI $\lambda\lambda 1032, 1038$ doublet) and then decreases further as OVI recombines. Heckman et al. (2002) pointed out that this allows us to substitute the values of f_{OVI} and t_{cool} at the OVI peak in equation (1), yielding

$$N_{\text{OVI}} \approx 10^{14} \left(\frac{v_g}{50 \text{ km s}^{-1}} \right) \text{ cm}^{-2} \quad (3)$$

for enriched gas; note that the result is independent of metallicity and physical density. The column density depends *only* on shock velocity ($N_{\text{OVI}} \propto T_s^{1/2}$) in this regime. However, comparison to the non-equilibrium postshock-cooling models of Dopita & Sutherland (1996) suggests that our prescription underestimates N_{OVI} by about a factor of two for most temperatures. This is particularly important for our low-density IGM absorbers: the recombination times for the ions and environments of interest can be comparable to (or even exceed) the age of the universe. For example, at $\Delta = 100$ and $T = 10^6\text{--}10^7 \text{ K}$, we find from Cloudy that (for these three ions) the typical radiative recombination times are, in most cases, only a few times smaller than the Hubble time. We therefore suggest that detailed shock models will be required for careful quantitative fits to the observations, especially if some shocks occur at lower densities.

The key assumption of this prescription is that the gas can cool past $T \approx 10^{5.45} \text{ K}$. While that is certainly true for most of the systems Heckman et al. (2002) considered (such as OVI in galactic winds), it is only marginally satisfied by IGM absorbers. Even at the OVI peak, $t_{\text{cool}} > H_0^{-1}$ for $Z \lesssim 0.05 Z_\odot$, and, because metal lines dominate the cooling at $10^5 \text{ K} \lesssim T \lesssim 10^{6.5} \text{ K}$, it increases rapidly above $T \sim 10^{5.5} \text{ K}$ as more and more atoms are ionized. Thus, tenuous, metal-poor gas and gas shocked to high temperatures will *not* be able to cool through the OVI peak, and the Heckman et al. (2002) argument actually only provides an upper limit to column densities in the IGM. To account for this possibility, we must limit the time over which gas cools to be smaller than H_0^{-1} . We let $T_{\text{min}} \equiv T_s[1 - (H_0 t_{\text{cool}})^{-1}]$ be the (approximate) temperature to which the gas cools, where the cooling time is evaluated at T_s and $T_{\text{min}} = 0$ if $t_{\text{cool}} < H_0^{-1}$. We then take f_{OVI} to be equal to its maximum value in the range (T_{min}, T_s) . For equation (1), we evaluate the cooling time at this effective temperature. If it exceeds the age of the universe, we instead substitute H_0^{-1} . We note that the

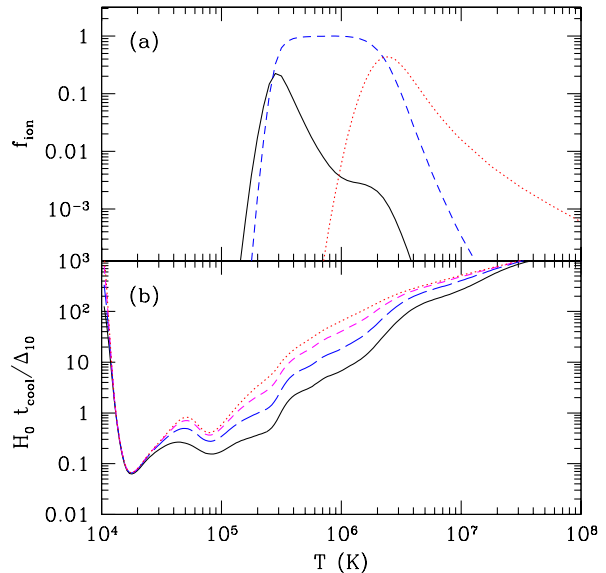


Figure 1. (a): Fractional abundance of OVI, OVII, and OVIII (solid, dashed, and dotted curves, respectively) if we assume CIE. (b): Ratio of the cooling time to the Hubble time, as a function of gas temperature. The solid, long-dashed, short-dashed, and dotted curves assume $Z = 0.3, 0.1, 0.03$, and $0.01 Z_\odot$, respectively. All curves assume that the gas element has density ten times the mean (i.e., $\Delta \equiv 10\Delta_{10}$, with $\Delta_{10} = 1$).

solution is more uncertain when $t_{\text{cool}} > H_0^{-1}$, because the density and metallicity of the gas do affect the total column density.

We illustrate these features in Figure 2. The thick curves show the column density of OVI as a function of shock temperature for a range of absorber metallicities and densities. We emphasize that the maximum N_{OVI} is nearly constant when $t_{\text{cool}} < H_0^{-1}$. However, for small density or metallicity and for large T_s , $N_{\text{OVI}} \propto \Delta Z$. Thus if OVI absorbers correspond to shocked regions, we expect a characteristic maximum $N_{\text{OVI}} \approx 10^{14} \text{ cm}^{-2}$. This is only approximate for (at least) two reasons. First, the viewing angle relative to the shock plane will smear out the sharp maximum. Second, as described above, detailed non-equilibrium calculations show that the column densities may be somewhat larger than we predict (by a factor of ~ 2 ; Dopita & Sutherland 1996). The crucial point is that the distribution of column densities should depend on the distribution of shock temperatures in the IGM. Its maximum is relatively robust to the choice of density and metallicity, but the abundance of weak absorbers can be quite sensitive to those values.

Of course, this postshock-cooling model does not just apply to OVI. As Heckman et al. (2002) pointed out, it also predicts that a range of ionization states should appear and disappear as the gas cools. Here we will focus on OVII and OVIII, whose detection with X-ray telescopes has received a good deal of attention. Naively comparing f_{OVI} and f_{OVII} in Figure 1a implies that *every* OVI absorber associated with a shock must also have a large N_{OVII} (although the converse is not true). We can use the same procedure as in equation (1) to estimate the column density as a function of temperature. The prescription is actually somewhat simpler because f_{OVII} is essentially flat. On the other hand, f_{OVIII} is large only if $T_s \gtrsim 10^{6.5} \text{ K}$, where $t_{\text{cool}} \gg H_0^{-1}$. Thus we do not expect OVI absorbers to host strong associated OVIII absorption, and vice versa. Note that this is one important difference between our (time-

¹ The CIE cooling models of Sutherland & Dopita (1993) are often used for this purpose. However, those tables modify the [O/Fe] ratio as a function of metallicity; because oxygen is particularly important for our purposes, we have chosen to keep its abundance fixed relative to other metals. For consistency with previous work, we use the solar-abundance ratios of Sutherland & Dopita (1993), with the exception of helium (which we set to its primordial value for a mass fraction $Y = 0.24$).

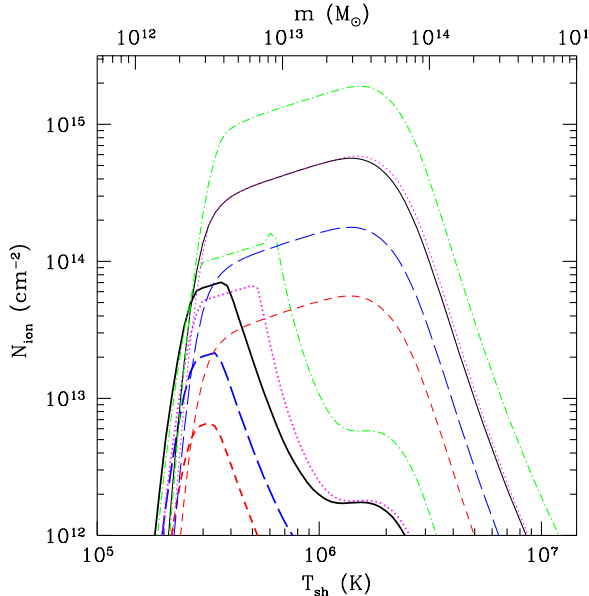


Figure 2. Column density of cooling material corresponding to a given shock temperature. The lower set of thick lines are for OVI, while the upper thin lines are for OVII. Solid, long-dashed, and short-dashed curves have $\Delta = 10$ with $Z = 10^{-1}, 10^{-1.5}$, and $10^{-2} Z_\odot$, respectively. Dot-dashed and dotted curves have $\Delta = 100$ with $Z = 10^{-1.5}$ and $10^{-2} Z_\odot$. The top axis shows the halo mass we associate with each infall shock (see §3.2).

limited) model and the fully-cooled predictions of Heckman et al. (2002). Of course, OVII and OVIII can coexist in the same system.

The thin curves in Figure 2 show the OVII column densities corresponding to each shock temperature. We see that OVII absorption should be significant over a much larger range of temperatures than OVI, but because the cooling times are long, the maximum N_{OVII} is much more sensitive to the gas density and metallicity. We therefore cannot robustly predict a maximum N_{OVII} . On the other hand, note that N_{OVII} is almost always several times larger than N_{OVI} , even near the OVI peak.

The postshock-cooling model also predicts physical sizes corresponding to each column: $\ell \approx v_g t_{\text{cool}} \approx 500 (v_g/50 \text{ km s}^{-1}) (H_0 t_{\text{cool}}) \text{ kpc}$. (Note that the last factor cannot exceed unity in our time-limited picture.) It is possible that geometric effects (such as the filamentary structure of the cosmic web) could provide more stringent constraints on the sizes (and hence column densities) of the absorbers. Also, note that when the cooling time is long, the density profile of the gas behind the shock can affect the column density (i.e., the assumption of a constant density medium may not be appropriate).

3 THE ABUNDANCE OF OXYGEN ABSORBERS

If the WHIM gas and the oxygen absorbers are a result of structure formation, it is natural to associate them with virialized dark-matter halos. We will suppose that each halo has a cross-section to host an absorber that is proportional to the square of its virial radius r_{vir} , which we will define as in Barkana & Loeb (2001). We can motivate such a scenario by noting that each halo is surrounded by a virial shock that heats accreting material to the virial temperature T_{vir} . Massive galaxy groups and clusters thus have a hot gas reser-

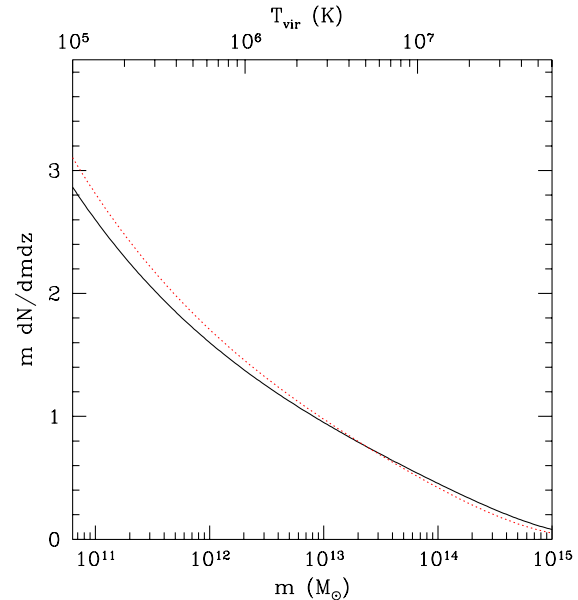


Figure 3. Number of virialized objects intersected per unit redshift as a function of halo mass. The top axis shows the corresponding virial temperature. The solid and dotted curves are for $z = 0$ and $z = 0.2$, respectively.

voir within r_{vir} . With this picture, we can compute the differential number dN/dz of absorbers per unit redshift via

$$\frac{dN}{dz} = \int dm n(m) \pi r_{\text{vir}}^2 \frac{dr}{dz}, \quad (4)$$

where all quantities are in comoving units. Here $n(m)$ is the Sheth & Tormen (1999) halo mass function. Figure 3 shows the integrand (weighted by mass m). The crucial result is that the number of systems intersected is small, of order a few per unit redshift. Thus, to reproduce the observed number density of OVI and OVII absorbers, we must have absorbers in the IGM outside of virial objects; however, the virialized systems could still account for strong absorbers, so we cannot neglect them entirely.

Moreover, we do not expect every halo to host an absorber of a given type. As the depth of the potential well increases, the virial shock becomes stronger and the gas temperature increases. Thus higher ionization states trace gas associated with larger objects, and we require some prescription to associate dark-matter halos with ion columns. We will now consider two simple possibilities: virial shocks and infall shocks.

3.1 Virialized Halos

Once gas falls through the virial shock, it is heated to T_{vir} and begins to cool radiatively. If t_{cool} is small, it accretes onto the central galaxy, passing through a range of ionization states along the way. If t_{cool} is large, the gas remains in a diffuse halo (White & Frenk 1991). Virial shocks thus provide an obvious source for hot absorbing gas.² The relevant halo masses can be read off from the top axis of Figure 3, which shows T_{vir} as a function of halo mass: we

² We note that both simulations and analytic arguments suggest that virial shocks do not form in many systems (Birnboim & Dekel 2003; Keres et al. 2004). However, for the halo masses and redshifts considered here, the “hot” accretion phase dominates and virial shocks should be omnipresent.

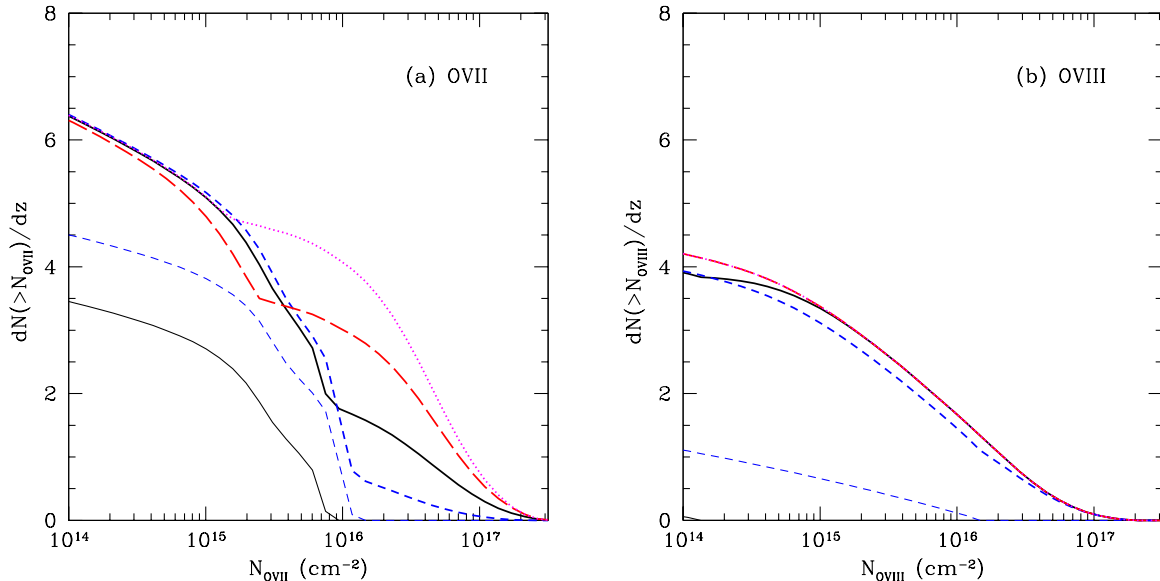


Figure 4. Number of virialized absorption systems with column density larger than some threshold per unit redshift for the OVII and OVIII ions (panels *a* and *b*, respectively) at $z = 0$. Long-dashed, solid, and short-dashed curves assume $Z = 0.03, 0.1$, and $0.3 Z_{\odot}$ with $\Delta_{\text{cool}} = 200$. The dotted curves assume $Z = 0.1 Z_{\odot}$ and $\Delta_{\text{cool}} = 50$. The thick curves show the total dN/dz , while the thin curves (plotted only for the solid and short-dashed cases) show the contribution from systems with $t_{\text{cool}} < H_0^{-1}$. In panel *b*, the dotted curve is coincident with the long-dashed curve and the thin solid curve is zero everywhere.

see that massive galaxies and groups correspond to the temperature range of interest.

To compute the absorber statistics, we will follow the simple picture of White & Frenk (1991) and divide the gas into two components. First, if $t_{\text{cool}} < H_0^{-1}$, we assume that it cools fully. We evaluate the cooling time at a density Δ_{cool} (usually 200) reflecting the typical density within a halo. In this case, we can compute the column density of each system using the postshock cooling model described in §2: each halo mass then corresponds to a single column density independent of the impact parameter (at least if we neglect orientation effects). Equation (4) gives the number of absorbers per unit redshift provided that we include only those halos hosting absorbers of the specified column. From Figure 1*b*, it is obvious that at virial overdensities, cooling will be complete for halos with $T_{\text{vir}} \lesssim 10^6$ K. This regime will thus be especially important for the OVI absorbers.

In the other regime, where $t_{\text{cool}} > H_0^{-1}$, the gas settles into a quasi-equilibrium hot halo with $T \approx T_{\text{vir}}$. We could again use the model of §2 to compute the corresponding columns. However, the density structure is likely to be important for virialized halos, and reasonably well-motivated models for the profile do exist. We will therefore use a simplified version of Perna & Loeb (1998), in which we integrate along a line of sight through the halo to find the column density; obviously the column density does depends on the impact parameter in this case. We will assume that a fraction $f_h = 0.5$ of an object's baryonic mass is contained in a diffuse gaseous halo within r_{vir} . We will also assume that its density follows a beta-model distribution, $\rho \propto [1 + (r/r_c)^2]^{-1}$, where r_c is the core radius. We will take $r_c = r_{\text{vir}}/4 \equiv c_{\beta} r_{\text{vir}}$, which is approximately consistent with the profiles of luminous clusters (Jones & Forman 1999). We will assume isothermal gas, so the col-

umn density N_{ion} along a line of sight with impact parameter b is

$$N_{\text{ion}} = f_{\text{ion}} Z [\text{O/H}]_{\odot} f_h \frac{2\Delta_c \bar{n}_H(z)}{3\Omega_m g(c_{\beta})} \frac{r_c}{\sqrt{1 + b^2/r_c^2}} \times \tan^{-1} \left(\sqrt{\frac{r_{\text{vir}}^2 + b^2}{r_c^2 + b^2}} \right), \quad (5)$$

where the metallicity is in solar units, Δ_c is the virialization overdensity in units of the critical density (Bryan & Norman 1998), and $g(x) = x^2(1 - x \tan^{-1} x^{-1})$. In the slow-cooling limit, we have $N_{\text{ion}} \propto f_h Z$. The number of systems per unit redshift is then the analog of equation (4),

$$\frac{dN(>N_{\text{ion}})}{dz} = \frac{dr}{dz} \int dm n(m) \pi R^2(m, N_{\text{ion}}), \quad (6)$$

where $R(m, N_{\text{ion}})$ is the maximum impact parameter for a halo of mass m within which the column exceeds N_{ion} .

Thus, to compute the total number of absorbers from virialized halos, we begin by dividing halos into fast-cooling and slow-cooling regimes (this amounts to finding the halo mass above which t_{cool} exceeds the age of the universe). For masses above this threshold, we approximate the halo as isothermal and use the halo mass profile of equation (5) to convert to column density as a function of impact parameter; the abundance is then given by equation (6). We need not specify a maximum halo mass, because $n(m)$ falls exponentially fast beyond the nonlinear mass scale. For smaller masses, the column density is determined by the shock physics of equation (1) *independent* of impact parameter, and the corresponding cross-section is given by equation (4) if we integrate only over those halos with sufficiently large columns. In this case, the integral converges because small halos correspond to small virial temperatures for which highly-ionized oxygen is vanishingly rare (see Fig. 2).

We show our results for OVII and OVIII in Figure 4. The

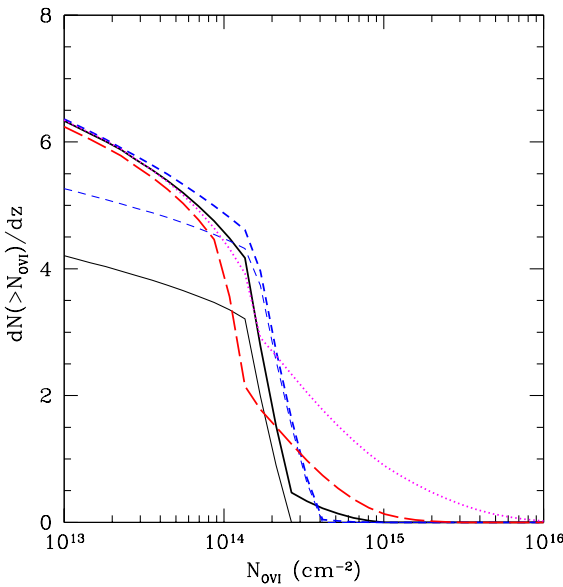


Figure 5. Same as Fig. 4, except for OVI.

thick curves show the total dN/dz , while the thin curves show the contribution from systems with $t_{\text{cool}} < H_0^{-1}$. Long-dashed, solid, and short-dashed curves assume $Z = 0.03, 0.1$, and $0.3 Z_{\odot}$ with $\Delta_{\text{cool}} = 200$. The dotted curves assume $Z = 0.1 Z_{\odot}$ and $\Delta_{\text{cool}} = 50$. As expected from Figure 3, the number of virialized absorbers is a few per unit redshift, well below the total frequency found in observations (Nicastro et al. 2005) and simulations (Fang et al. 2002) but consistent with other analytic treatments of virialized objects (Perna & Loeb 1998). Systems with $t_{\text{cool}} < H_0^{-1}$ can make a significant contribution to the OVII absorbers but are unimportant for OVIII. However, they are always relatively weak, with a characteristic $N_{\text{OVII}} \sim 10^{15.5} \text{ cm}^{-2}$ (that is relatively independent of metallicity). In contrast, hot halos can contain quite large columns, because the path lengths can be long. The abundance of OVII absorbers is larger than that of OVIII because halos near the nonlinear mass scale have $T_{\text{vir}} \lesssim 10^{6.5} \text{ K}$, below the ionization threshold of OVIII.

Note that the number of high-column-density absorbers *increases* if the metallicity decreases. As the metallicity declines, the cooling time increases and less-massive halos retain their hot gas. This makes up for the decreased column in any one absorber because $n(m)$ falls rapidly with mass. This is in many respects an artifact of our simplified treatment: for $t_{\text{cool}} \sim H_0^{-1}$, we should include cooling to compute the detailed column densities.

Here and below, we present results for $z = 0$. The statistics evolve only modestly to $z \sim 1$ (e.g., compare the two curves in Figure 3). Beyond that, the abundance falls rapidly because the nonlinear mass scale falls below $T_{\text{vir}} \sim 10^6 \text{ K}$.

Figure 5 shows analogous results for OVI. In this case, the rapidly-cooling halos are even more important, yielding a characteristic column density $N_{\text{OVI}} \sim 10^{14.5} \text{ cm}^{-2}$ (see Figure 2). The high- N_{OVI} tail is composed of halos just above the cooling threshold which still have relatively large f_{OVI} . Thus it only appears if the cooling time is long (i.e., Z or Δ_{cool} is small) and is subject to uncertainties in our simplified cooling model.

As required by Figure 3, virial shocks underpredict dN_{OVI}/dz and dN_{OVII}/dz by factors of several. Clumping will

further decrease the cross section. If we place the shocked gas into n_b blobs of radius $r < r_{\text{vir}}$, only a fraction $f_{\text{cov}} \approx n_b(r/r_{\text{vir}})^2 < 1$ of lines of sight through each halo would host absorbers. It could, however, increase the column densities. In the slow-cooling case, we would have $N_{\text{ion}} \propto f_{\text{cov}}^{-1}$, increasing the amplitude of the strong-absorber tail. On the other hand, fast-cooling gas would be unaffected.

Finally, we note that we have allowed the gaseous halos in groups to remain relatively dense and hot. It is well-known that such models overpredict the soft X-ray background (Pen 1999; Wu et al. 2001). One solution is to introduce a feedback mechanism that decreases the density of the intragroup medium (Wu et al. 2001; Xue & Wu 2003). This would, of course, modify our column-density distribution. By slowing the cooling, the principal effect would be to increase the amount of absorption. It could also slightly increase the cross section if the gas is spread over larger distances. However, simple geometry demands that such pre-heating scenarios will certainly not bring the abundance into agreement with observations; it is more likely to change the column densities by a modest amount. In principle, the distribution of strong IGM absorbers could then be used as a probe of feedback mechanisms, though the many other uncertainties (such as metallicity and non-equilibrium effects) make this a difficult endeavor.

3.2 Infalling Gas

To reproduce the large number of absorbers found in simulations and observations, we *must* appeal to a population beyond virial shocks. This is of course not surprising, because simulations contain large networks of IGM shocks. To connect these shocks with collapsed objects, we will postulate that the temperature T_{sh} of IGM shocks surrounding each dark-matter halo depends (exclusively) on the halo mass. One way to motivate such a picture is if the shocks occur during infall onto existing structures. Furlanetto & Loeb (2004) used this *ansatz*, together with spherical symmetry, to estimate the distribution of IGM shocks. They argued that shocks could plausibly occur when an object breaks off from the cosmological expansion (at “turnaround”), because that is the point at which the flows begin to converge. Assuming strong shocks, the peculiar velocity at turnaround implies $T_{\text{sh}} \approx T_{\text{vir}}/4$. The model roughly matches simulation estimates of the mass fraction and characteristic temperature of the WHIM. Although clearly a simplification, this picture does describe many of the major features of the WHIM and provides a well-defined way to convert $n(m)$ to the distribution of T_{sh} . Furthermore, spherical infall occurs on quite large scales and could provide the cross section we need. Turnaround occurs at $r_{\text{ta}} \approx 3.3r_{\text{vir}}$ for self-similar spherical infall (Bertschinger 1985) in an Einstein-de Sitter universe, so the shock networks could be quite large relative to collapsed objects. Simulations also show networks of shocks surrounding bound structures at a few times the virial radii (Keshet et al. 2003; Nagai & Kravtsov 2003). We will, however, leave the cross section of each infall shock free, because it must depend on the asymmetric, filamentary nature of the infall. We will parameterize it as $\chi\pi r_{\text{vir}}^2$. For reference, the top axis of Figure 2 shows $T_{\text{sh}}(m)$ in this infall model.

Because of the lack of data pertaining to IGM shocks, a detailed comparison of this model with observations is difficult. However, Rines et al. (2003) have used galaxy redshifts to trace the infall regions of eight nearby clusters spanning about an order of magnitude in mass. Although the galaxies obviously will not be subject to shocks, their structure should reflect the underlying

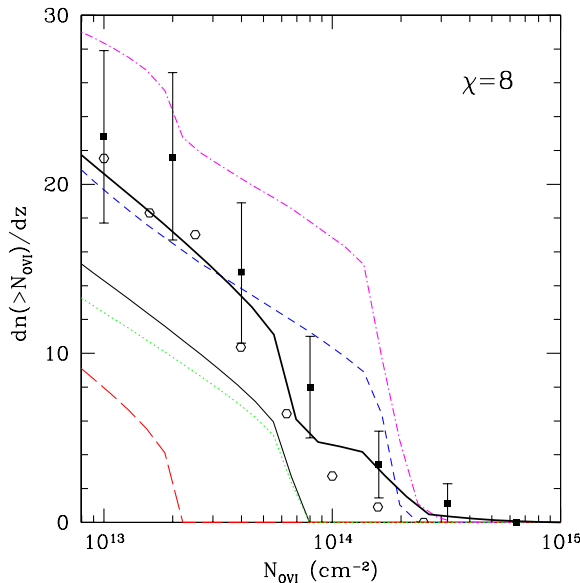


Figure 6. Number of absorption systems from infall shocks for the OVI ion at $z = 0$, assuming $\chi = 8$. The long-dashed, thin solid, and short-dashed curves assume $Z = 0.03, 0.1$, and $0.3 Z_{\odot}$, respectively, with $\Delta = 10$. The dot-dashed curve assumes $Z = 0.1 Z_{\odot}$ with $\Delta = 100$. The dotted curve is the same as the solid curve except that we take $T_{\text{sh}} = T_{\text{vir}}/6$. The two sets of points show observed results (the solid squares are described in the text; the open hexagons are from Danforth & Shull 2005). The thick solid curve adds the contribution from virialized systems.

gas distribution at least qualitatively. Most importantly, Rines et al. (2003) found that $r_{\text{ta}} \approx 3.5 r_{\text{vir}}$ in all of their clusters. The spherically-averaged density profiles fall as $\sim r^{-3} - r^{-4}$ at large radii, consistent with simulations (Hernquist 1990; Navarro et al. 1997). This implies that the average density falls by about a factor of fifty between the virial radius and turnaround radius. However, as we will show in §4 below, the density field is highly inhomogeneous within this region. For simplicity, we will assume a constant density behind these shocks. Finally, Rines et al. (2003) compute the velocity dispersion profiles. Between r_{vir} and r_{ta} , the dispersion typically declines by a factor of two or so. This is nicely consistent with our assumption that $T_{\text{sh}} \approx T_{\text{vir}}/4$.

Given this prescription, we can compute the expected number of absorbers using the postshock cooling model of §2. Here we will use this model for both fast-cooling and slow-cooling shocks, because (unlike for virialized halos) we have no well-motivated model for the density profile of IGM filaments. However, we caution the reader that geometry (such as the thickness of filaments) could still ultimately determine the column densities. We also note that, for these modest densities $\Delta \sim 10$, the recombination times can approach or even exceed the age of the universe, so our assumption of local CIE in calculating the abundances may be problematic (see discussion in §2). To compute dn/dz , we use equation (4), with the integration range set by the column density corresponding to each halo mass. Operationally, the calculation is similar to that described in §3.1, except that equation (1) applies to both fast and slow-cooling shocks.

Given the simplifications of our model, a detailed comparison to observations is unwarranted. However, we do wish to estimate the required χ as well as check whether the derived column densities are reasonable. As such, we begin with OVI, which is

by far the best studied ion. The filled squares in Figure 6 show a distribution compiled from several lines of sight in the literature (Tripp et al. 2000; Sembach et al. 2001; Richter et al. 2004; Prochaska et al. 2004); these lines of sight have the best-defined samples.³ We have included all claimed detections (even those labeled “tentative” by each survey’s authors). The error bars assume Poisson statistics. The open hexagons show the more systematic survey of Danforth & Shull (2005), who searched for OVI absorbers in 129 known Ly α absorbers along 31 lines of sight studied with the *FUSE* satellite. We refer the reader to that paper for a detailed discussion of the errors. Note that the two datasets are reasonably consistent, though the Danforth & Shull (2005) data do lie below our compilation by a small amount.

The curves in Figure 6 show the results from our model assuming $\chi = 8$. The long-dashed, solid, and short-dashed curves assume $Z = 0.03, 0.1$, and $0.3 Z_{\odot}$, respectively, with $\Delta = 10$. The dot-dashed curve assumes $Z = 0.1 Z_{\odot}$ with $\Delta = 100$. The dotted curve is the same as the solid curve except that we take somewhat weaker shocks, with $T_{\text{sh}} = T_{\text{vir}}/6$. The thick solid curve adds the contribution from virialized systems for a better comparison with the observations.

In all cases, the number of OVI absorbers falls sharply at some characteristic column density. This is simply the maximum allowed for fast-cooling shocks. In contrast to virial shocks, however, the densities are typically small enough that the maximum column density does depend on the metallicity and physical density (unless $Z \sim 0.3 Z_{\odot}$ or $\Delta \sim 100$, in which case the cooling times begin to fall below the age of the universe). Below the characteristic maximum, the number of absorbers rises rapidly because f_{OVI} is so sensitive to the shock temperature. We thus expect infall shocks to contribute only to the range $N_{\text{OVI}} \lesssim 10^{14} \text{ cm}^{-2}$. Note that the sharp rise in the dot-dashed curve at $N_{\text{OVI}} \approx 2 \times 10^{13} \text{ cm}^{-2}$ occurs because of the plateau in f_{OVI} at $T \sim 10^6 \text{ K}$ (see Fig. 1). Of course, the maximum N_{OVI} does not decrease for $T_{\text{sh}} = T_{\text{vir}}/6$ because that has no effect on the cooling. It decreases dN/dz by a small amount because it shifts the halo mass corresponding to each T_{sh} .

Thus, if all the known absorbers are to be attributed to shocks (either infall or virial), we find that $\chi \sim 8$; i.e., the infall shocks subtend an area eight times larger than the halo itself. While large, this is smaller than the expectation from pure spherical infall so may not be unreasonable. Moreover, as we will discuss in §5 below, a number of the observed systems appear to be photoionized and have a different origin, which would allow the covering factor of infalling gas to decrease by about a factor of two. This would decrease the thin curves in Figure 6 by the same factor: note that we would still expect a sharp decline near the characteristic maximum column density of the shocks. Because stronger systems only arise in virial shocks, the covering fraction within virialized objects can be separately calibrated from the abundance of strong absorbers (though of course that could also be a function of halo mass). In the simplest model, a significant population of photoionized absorbers would fix $\chi \approx 4$, allowing IGM absorbers to be more filamentary, while leaving the virial shock spherical. In any case, we find it reassuring that a reasonable choice for χ can simultaneously match the observed abundance and column-density distribution, at least roughly.

³ However, we have not attempted to account for the different detection limits of each survey. As such, the statistics at $N_{\text{OVI}} \sim 10^{13} \text{ cm}^{-2}$ may not be reliable.

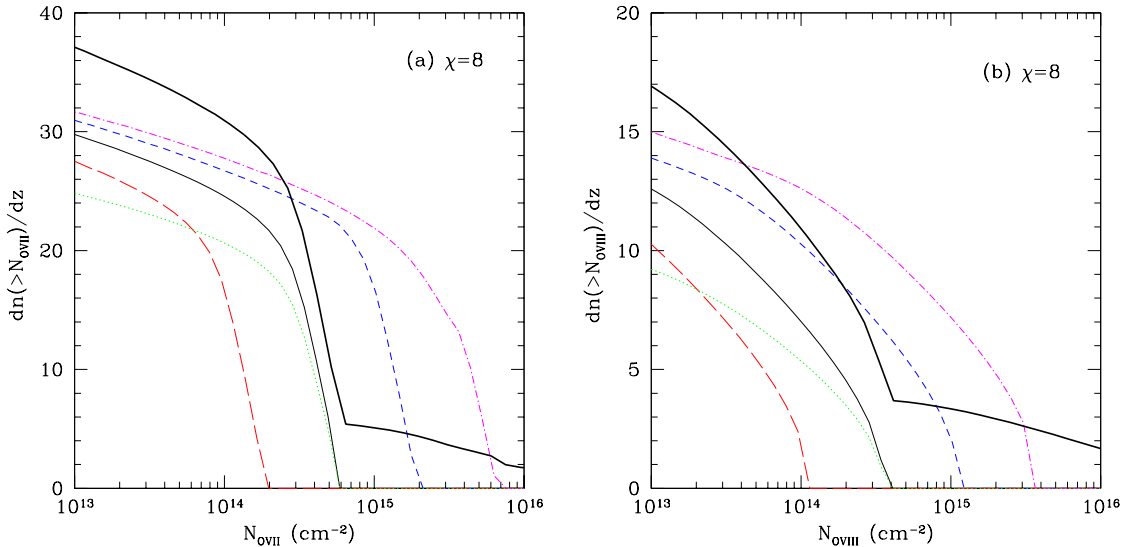


Figure 7. Same as Fig. 6, except for the OVII and OVIII ions (panels *a* and *b*, respectively). Note that the ordinates have different scales.

We repeat the same exercise for OVII and OVIII in Figure 7. We have again fixed $\chi = 8$. First, note that the number and characteristic columns of OVII absorbers are much larger than for OVI absorbers. This follows easily from Figure 2, because OVII dominates over a much larger temperature range (including the OVI peak). On the other hand, the maximum N_{OVII} is poorly constrained: because the cooling times always exceed the age of the universe, the cutoff is proportional to metallicity and density. Interestingly, OVII drops off steeply at this maximum and is nearly flat below it, so most absorbers of a given metallicity and density should cluster around one particular column. This occurs because every system cools over H_0^{-1} and f_{OVII} is nearly independent of temperature. In reality, the cutoff will be smeared by the range of metallicity and density as well as geometry. For X-ray lines, the comparison to observations is much more difficult given current technology. There is only one well-studied line of sight (with secure detections of two absorbers); formally this implies $dN/dz(N_{\text{OVII}} \gtrsim 7 \times 10^{14} \text{ cm}^{-2}) = 67^{+88}_{-43}$ (Nicastro et al. 2005). Our model is well within this range. More interesting is to note that the observed columns (7×10^{14} and 10^{15} cm^{-2}) are both near the cutoff and appear to require $\Delta \gtrsim 30$ or $Z \sim 0.3 Z_\odot$, still well within reasonable bounds. Simulations suggest $dN/dz(N_{\text{OVII}} \gtrsim 7 \times 10^{14} \text{ cm}^{-2}) \sim 10-30$, close to our model with $\chi = 8$ (Fang et al. 2002; Chen et al. 2003). They do not show as severe a break as our model, probably because of scatter in the metallicity and geometric effects.

Figure 7b shows that the expected number of OVIII absorbers is about half that of OVII, although the column densities can be comparable. OVIII is rarer simply because the characteristic shock temperature is $\lesssim 10^{6.5} \text{ K}$ (Furlanetto & Loeb 2004), so there is not as much gas with large f_{OVIII} . As a result, virialized systems make a larger relative contribution. Also, note that OVIII does not show a sharp cutoff; this is because f_{OVIII} varies rapidly with temperature.

4 COMPARISON TO SIMULATIONS

We have shown that the spherical-infall model described in the previous section can explain many of the key properties of the absorbers. However, it also makes a number of important assumptions and simplifications. Here we compare our model to simulations in order to highlight its strengths and weaknesses.

4.1 The Cosmological Simulation

We use the $z = 0$ dark-matter, stellar-particle, gas-temperature and density outputs of a large scale $L = 25h^{-1}\text{Mpc}$ cosmological hydrodynamical simulation, with 768^3 fluid elements and 384^3 dark-matter particles (each with mass $2 \times 10^7 h^{-1} M_\odot$). The code structure is similar to that in Cen & Ostriker (1992a,b) with some significant changes (Cen & Ostriker 2000). It is described in detail in Nagamine et al. (2001). The chosen cosmology is the “concordance model” (Wang et al. 2000), a flat low-density ($\Omega_m = 0.3$) universe with a cosmological constant ($\Omega_\Lambda = 0.7$), and $h = 0.67$. The baryon density (originally $\Omega_b = 0.049$) has been scaled to $\Omega_b = 0.046$ to match the value used in our analytical model. The galaxy particles are formed through the recipe described in the Appendix of Nagamine et al. (2000). Each stellar particle is assigned a position, velocity, formation time, mass, and metallicity at birth. The stellar particle is placed at the center of the cell with a velocity equal to the mean velocity of the gas in the cell. It is then followed by a particle-mesh code as a collisionless particle interacting gravitationally with the dark matter and the gas. We use the galaxy and group position information obtained from these stellar particles by Nagamine et al. (2001).

We will primarily be concerned with the IGM around bound objects. We use the dark-matter halo parameters for this simulation obtained by Nagamine et al. (2001) with the HOP grouping algorithm of Eisenstein & Hu (1998). We then search for the halos that are most closely coincident ($\Delta L \leq 68 h^{-1} \text{ kpc}$) with the galaxy-particle groups and use the properties of these dark-matter halos. The virial radius is obtained from halo mass using equation (24) of Barkana & Loeb (2001). Around the center of each halo, we

obtain the volume-averaged radial distributions of matter, temperature, and metals in the inner regions abutting the galaxy-particle locations in the $z = 0$ output:

$$\frac{\int d^3x \rho(x) Q(x)}{\int d^3x \rho(x)}, \quad (7)$$

where $Q(x)$ is the parameter value (Δ , T , f_{ion} , etc.) in the volume element d^3x . For the sake of transparency, we do not directly use the metallicities reported by the simulation. Instead we consider two metallicity prescriptions. The first scales metallicity with density as described by Croft et al. (2001), $Z = 0.005 Z_{\odot} \times \sqrt{n/\bar{n}}$, with a maximum metallicity of $Z = 0.33 Z_{\odot}$. The second prescription simply uses a constant metallicity $Z = 0.1 Z_{\odot}$. In order to study the OVI, OVII, and OVIII abundance distributions, we compute the ionization fraction as a function of temperature as illustrated in Figure 1a. With f_{ion} for each cell, plus the density and metallicity, we compute the total ionic abundance relative to hydrogen. We scale the distributions by the virial radius corresponding to each halo and follow them out to five virial radii. We obtain the volume-averaged distributions for several virial-radius bins, $r_{\text{vir}} = 240\text{--}300$, $360\text{--}480$, and $600\text{--}720$ kpc; these correspond to roughly (1–2), (3–7), and $(14\text{--}24) \times 10^{12} M_{\odot}$.

4.2 Absorbers Around Virialized Halos

The key *ansatz* in our infall-shock model is that the characteristic IGM temperature surrounding a collapsed object increases with its mass, even on scales much larger than r_{vir} . Figure 8 shows spherically-averaged temperature profiles around halos in the simulation (normalized by r_{vir}).⁴ We see that isolated galaxies tend to lie in cooler regions of the IGM than massive groups, even at several times r_{vir} . The trend appears to break down at $r \gtrsim 3r_{\text{vir}}$ for the smallest objects. This is in a temperature range where cooling can be significant, which may affect the results. Also note that there is no characteristic radius at which the temperature increases, as would be expected for pure spherical infall. Thus the shocks appear to be complex and distributed, with a range of temperatures. The typical temperature is, however, a few times smaller than T_{vir} , consistent with our model.

Figure 9 shows that it may be more accurate to associate different oxygen ions with different halo masses. The three panels show the spherically-averaged ionization fractions for each of our ions as a function of normalized radius. The curves correspond to the same mass ranges shown in Figure 8. We see that OVI tends to be associated with the smallest-mass objects, although even these halos are too hot to sustain a large f_{OVI} inside r_{vir} . On the other hand, OVIII is most prevalent around the highest-mass objects (although not within the virialized regions, again because the gas is too hot) and is extremely rare around the low-mass objects. Finally, OVII appears in all systems because it dominates over such a wide temperature regime; only the virialized gas in extremely massive objects is hot enough to destroy OVII.

Thus, we can be confident in expecting highly-ionized absorbers to lie near massive collapsed objects. However, the simulations also show that a simplified spherical model is not accurate. In Figure 10 we have computed dn/dz for each ionic absorber using our spherical profiles. We have used equation (6) with the column densities determined by integrating through the average profiles.

⁴ At $r \ll r_{\text{vir}}$, the temperature is strongly affected by star formation and feedback, so we will ignore that portion.

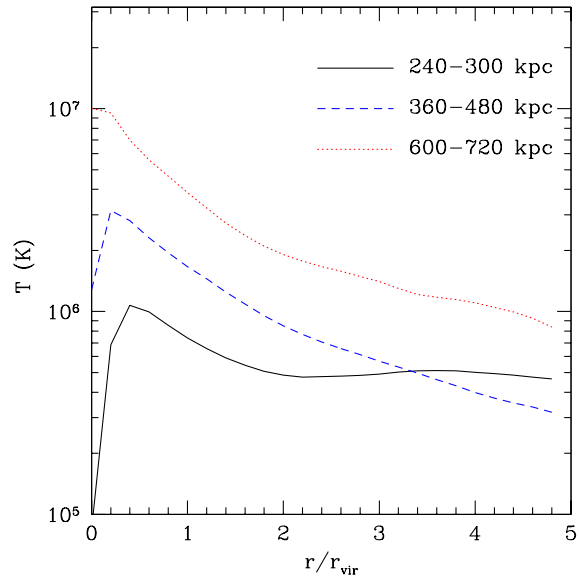


Figure 8. Spherically-averaged temperature profiles around virialized halos in a cosmological simulation, where all distances are scaled to the virial radius. The three curves show different mass ranges.

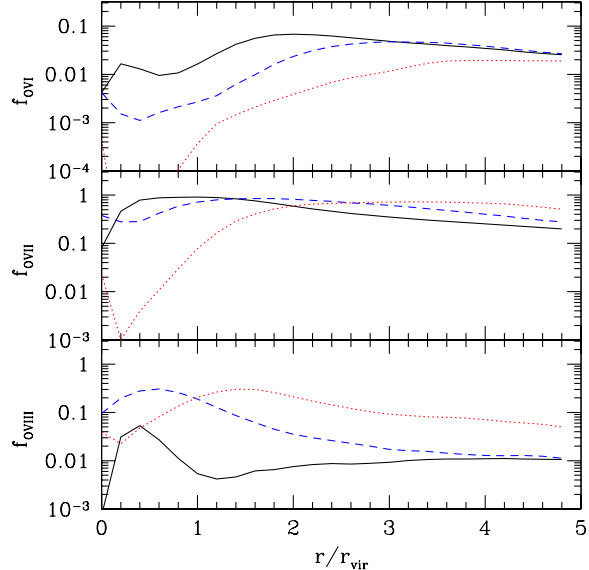


Figure 9. Spherically-averaged ionization fractions around virialized halos in a cosmological simulation, where all distances are scaled to the virial radius. The top, middle, and bottom panels are for the OVI, OVII, and OVIII ions. In each panel, the three curves show different mass ranges, as in Fig. 8.

In each case we truncate the profile at $5r_{\text{vir}}$. The dotted, dashed, and solid curves show the expected statistics for OVI, OVII, and OVIII, respectively. First consider the thin curves, which assume a constant $Z = 0.1 Z_{\odot}$ metallicity (as in our fiducial analytic model). We see $dn/dz \sim 65$ for each ion at sufficiently small column densities. This is an artifact of truncating the integrating at $5r_{\text{vir}}$. The profiles in Figure 9 tend to approach nearly constant values at large radii, so for large impact parameters the column density

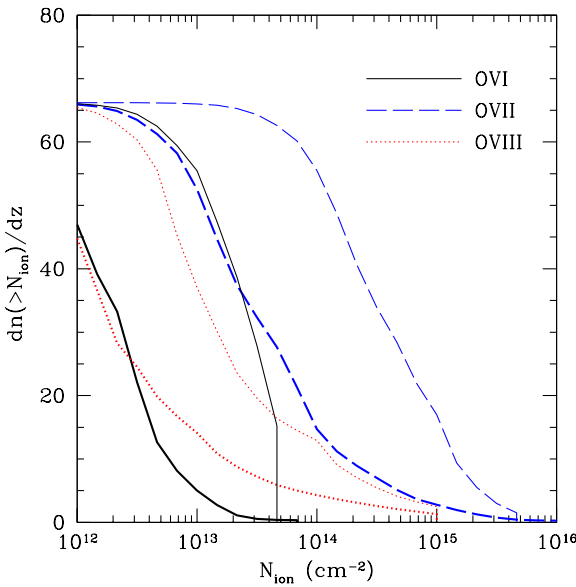


Figure 10. Absorber statistics for spherically-averaged profiles taken from the simulations. The different line styles show the three different ions. The thin curves assume a uniform $Z = 0.1 Z_{\odot}$ metallicity; the thick curves use a density-dependent metallicity prescription (see text).

is essentially proportional to the maximum radius; only well above this turnover can the column densities be trusted.

In that range, OVII and OVIII do not present dramatically different pictures from the analytic model. Because f_{OVII} is nearly temperature-independent over a broad range, we might expect spherical averages to do a passable job with that ion. Indeed, the number density does agree roughly with our model and with more detailed simulation analyses (Fang et al. 2002; Chen et al. 2003). But it is certainly not so good that we can claim support for our model. OVIII is considerably worse, and the OVI results do not appear to have converged and disagree strongly with our model. This is also not surprising, because OVI is often in a fast-cooling regime and is so temperature sensitive that averaging over large volumes artificially suppresses its importance. Ray tracing appears vital to predict the OVI absorber abundance, as would be expected in a shock-cooling model.

The thick curves in Figure 10 assume the density-dependent metallicity distribution described above. The number of absorbers declines sharply in this scenario: at large radii the mean physical densities are near the cosmic mean, so the overall metallicity is small. As a result, high column densities require small impact parameters. One fortunate consequence is that the curves converge better. However, much more significantly, the number of absorbers is far below the result of more complete simulation analyses (Cen et al. 2001; Fang & Bryan 2001; Fang et al. 2002; Chen et al. 2003). Thus, the spherical averages do not accurately describe the absorbers in simulations. Of course, the reason is the clumpiness of the IGM.

Figure 11 shows phase diagrams of the IGM gas surrounding halos with $M = 3-7 \times 10^{12} M_{\odot}$ in four radial slices. The n_{OVI} , n_{OVII} , and n_{OVIII} -averaged contours were obtained using the Croft et al. (2001) prescription for the metallicity. Hotter gas tends to sit at higher densities (and hence occupy a small volume). This correlation holds even at $\Delta \sim 1-10$, well below virial over-

densities. Moreover, the mean temperature and density decrease and the scatter in the relation increases as one moves away from the central galaxy. However, regardless of radius there is a non-negligible fraction of gas at high temperatures comparable to T_{vir} . This gas (which also has a relatively large density) is presumably responsible for most of the oxygen absorption. Thus, as can be seen from Figure 11d, the higher-ionization states will tend to probe the densest filaments (and the most enriched gas, on average) around each structure, in addition to the largest structures. Meanwhile most of the volume is filled with cooler, low-density gas that has a small metallicity given our prescription. The averaging procedure smooths the high-density gas, boosting the column density along all lines of sight under a constant metallicity. But when the metallicity is density-dependent, the tenuous gas is so metal-poor that the dense clumps essentially disappear during averaging. These clumps are reflected in the fragmentary nature of the density-averaged contours at higher Δ . As one moves outward, they represent an ever decreasing fraction of the volume but continue to contribute significantly to n_{OVII} , n_{OVIII} , and even n_{OVI} . The distribution is highly complex: there is a wide range of temperatures for any given density (spanning about a decade for $\Delta \sim 10$), which reflects the non-uniformity of the infall process.

How can we reconcile the apparent success of our analytic treatment with the clear failure of spherical averaging in simulations? The key reason is that, with the exception of hot virialized halos, we did not use spherical geometry in the calculation; instead we used only the infall velocities and a cooling time (capped at H_0^{-1}). The physics of shock cooling then predicted the column densities without recourse to the gas distribution. Thus we only need modify our picture to describe a network of inhomogeneous shocks with total cross section $\pi\chi r_{\text{vir}}^2$ rather than a single coherent structure. Of course, it is still an open question whether our model provides an accurate description of these networks even on a mean level (specifically the shock temperature). In the future, quantitative treatments must also consider the importance of the scatter seen in Figure 11.

5 PHOTOIONIZED GAS

To this point, we have focused on systems that are cooling after being collisionally ionized by a shock. In simulations, such systems make up only about half of the OVI absorbers (Cen et al. 2001; Fang & Bryan 2001). The others are photoionized; such systems are rare for the strong absorbers but dominate at $N_{\text{OVI}} \sim 10^{13} \text{ cm}^{-2}$. In the simulations, these absorbers are typically cooler and lower density than collisionally-ionized systems. Modeling of the observed OVI systems also suggests that about half are photoionized (e.g., Prochaska et al. 2004). However, this interpretation is subject to uncertainties in the relative metal abundances, the ionizing background, and whether the medium is multiphase. Reliably separating this population is crucial because it typically has $T \sim 10^4 \text{ K}$, which means that these systems are not part of the canonical WHIM. We have shown in §2 (see Fig. 2) that post-shock cooling predicts that individual OVI absorbers should have OVII columns about an order of magnitude larger than N_{OVI} . This is larger than $f_{\text{OVI}}/f_{\text{OVII}}$ in CIE at the OVI peak because most shocks begin at higher temperatures and cool into the OVI range, so OVII probes a longer path length through the postshock region. We now calculate the associated OVII columns if photoionization dominates.

We have again used Cloudy (version 94, Ferland 2001) to

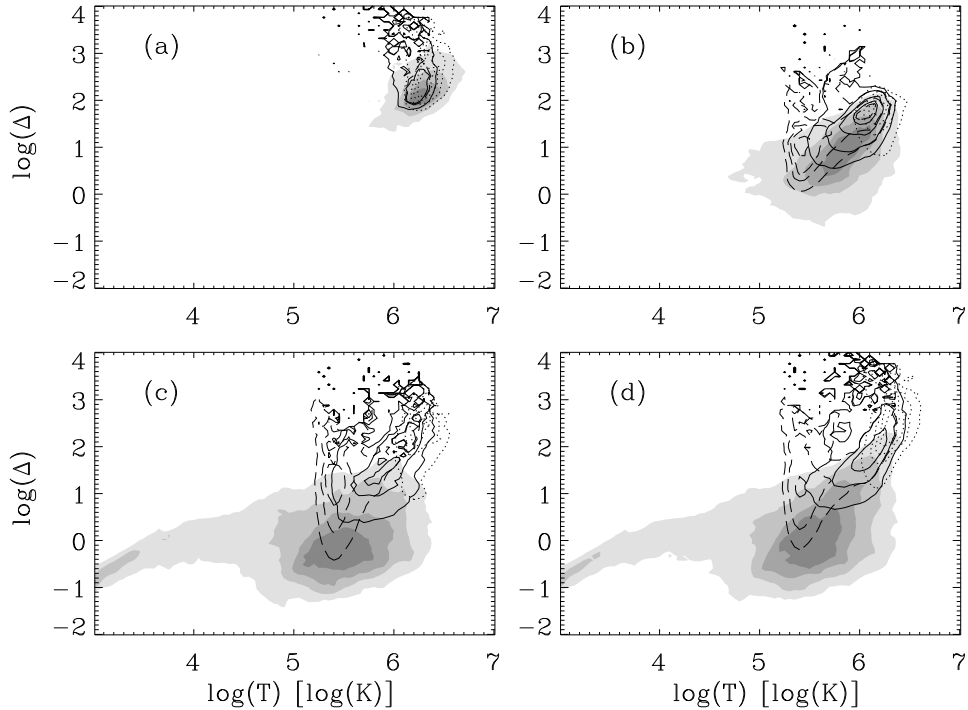


Figure 11. Contour plots, in the density-temperature plane, of the volume-weighted (grey-scale), n_{OVI} -weighted (dashed), n_{OVII} -weighted (solid), and n_{OVIII} -weighted (dotted) distribution of gas within $0-1r_{\text{vir}}$ (panel *a*), $1-3r_{\text{vir}}$ (panel *b*), $3-5r_{\text{vir}}$ (panel *c*), and $0-5r_{\text{vir}}$ (panel *d*) of halos with $r_{\text{vir}} = 360-480$ kpc (or $M = 3-7 \times 10^{12} M_{\odot}$). The contours enclose 0.95, 0.75, 0.5 and 0.25 of the total volume or ion number.

compute f_{OVI} and f_{OVII} assuming ionization equilibrium with an input radiation background. We constructed a grid in density and temperature with spacings $\Delta \log n_H = 0.5$ for $-7 < \log n_H < -3$ (in units of cm^{-3}) and $\Delta \log T = 0.1$ for $3 < \log T < 7$ (in K). We use the $z = 0$ Haardt & Madau (2001) ionizing background normalized to a total ionizing rate $\Gamma_{-12} = 0.084$ (in units of 10^{-12} s^{-1}). This roughly matches the observational estimate of Davé & Tripp (2001).

Figure 12 summarizes our results. Panel (*a*) shows the logarithm of the ratio $f_{\text{OVI}}/f_{\text{OVII}}$. Dashed (solid) contours indicate $f_{\text{OVI}}/f_{\text{OVII}} > 1$ (< 1). To delineate those regions of phase space where we could expect OVI absorbers in the IGM, panel (*b*) shows the logarithm of the path length (in kpc) that would be required to produce an absorber with $N_{\text{OVI}} = 10^{13} \text{ cm}^{-2}$ if $Z = 0.1 Z_{\odot}$. Systems with $L \lesssim 100$ kpc are confined to gas with $T \lesssim 10^{5.5}$ K and $n_H \sim 10^{-6}-10^{-4} \text{ cm}^{-3}$ or to relatively dense gas lying close to the ionization temperature of OVI. In the former case, we find that $f_{\text{OVI}}/f_{\text{OVII}} \gtrsim 1$, unless the gas has $T \sim 10^{5.45}$ K (in which case collisional processes dominate and it is part of the WHIM) or is extremely tenuous and spatially large. Thus, photoionized absorbers have smaller associated X-ray absorption than in the postshock cooling model and comparison of $f_{\text{OVI}}/f_{\text{OVII}}$ offers a powerful test of the nature of the absorbing gas. Upper limits of $N_{\text{OVII}} \sim 3N_{\text{OVI}}$ can robustly identify those absorbers with $T < 10^5$ K and separate WHIM systems from cooler photoionized gas.

This conclusion holds even if the ionizing background has a different amplitude or shape. The ratio $f_{\text{OVI}}/f_{\text{OVII}}$ is nearly independent of Γ_{-12} . The required path length for low-density cool

gas increases slightly as Γ_{-12} increases, making tenuous absorbers more unlikely. The shape of the metagalactic background matters little since the ionization potentials of OV and OVI are so closely spaced (114.2 eV and 138.1 eV, respectively). We would have to introduce a (physically unmotivated) sharp feature to the background in this energy range to substantially change the ion ratios. We have verified this with the Haardt & Madau (1996) ionizing background, which includes only quasars and is significantly harder than the Haardt & Madau (2001) background (which also includes galaxies). The corresponding Figure 12 looks identical.

It is worth emphasizing that $f_{\text{OVI}}/f_{\text{OVII}}$ is less subject to modeling uncertainties than constraints that use only UV lines (e.g., Prochaska et al. 2004) because it depends only on a single atomic species. We also note that other ionization states could be useful. For example, shocks that produce OVIII have $t_{\text{cool}} \gg H_0^{-1}$ and should not contain substantial OVI. Thus a large measured $f_{\text{OVI}}/f_{\text{OVIII}}$ would help to identify photoionized systems. Note that Heckman et al. (2002) imply that large columns of OVI and OVIII can coexist in the same absorber. This is because they implicitly assume that the material cools fully; while reasonable for Galactic systems, this limit is not relevant for IGM absorbers.

Finally, Heckman et al. (2002) also pointed out that the linewidth—column-density relation offers another way to discriminate between photoionization and postshock cooling.

6 DISCUSSION

In this paper, we have attempted to elucidate the physical origin and properties of IGM oxygen absorbers (OVI, OVII, and

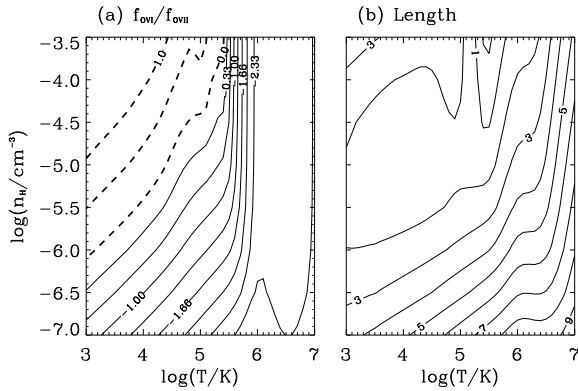


Figure 12. (a): Contours show $f_{\text{OVI}}/f_{\text{OVII}}$ as a function of gas density and temperature, assuming photoionization equilibrium in a $z = 0$ Haardt & Madau (2001) ionizing background with $\Gamma_{-12} = 0.084$. The dashed contours indicate $f_{\text{OVI}}/f_{\text{OVII}} > 1$ while the solid indicate $f_{\text{OVI}}/f_{\text{OVII}} < 1$; they are labeled with the logarithm of the ratio. (b): The path length required for a total column density $N_{\text{OVI}} = 10^{13} \text{ cm}^{-2}$ if the absorber has $Z = 0.1 Z_{\odot}$. The contours are labeled with the logarithm of the distance in kpc.

OVIII) with a set of simple analytic arguments. While simulations appear to predict approximately the correct number of absorbers (Cen et al. 2001; Fang & Bryan 2001; Fang et al. 2002; Chen et al. 2003), such studies have only examined the physical origin of the absorbing gas in a cursory fashion. We first argued that the typical maximum column density of OVI absorbers ($N_{\text{OVI}} \sim 10^{14} \text{ cm}^{-2}$) follows naturally from postshock cooling (Heckman et al. 2002), suggesting that at least some absorbers are generated by structure-formation shocks. We then argued that, if these shocks are associated with bound structures, we must have a (more numerous) population of significantly hotter shocks around larger objects. These shocks can be traced by OVII and OVIII; the former is more useful because it dominates over such a broad temperature range. Moreover, shocked OVI systems must all have strong OVII absorption. This contrasts with photoionized OVI absorbers, which should have OVII columns not much larger than the OVI columns.

We showed that a simple picture with virial shocks and “infall” shocks can account for the observed number density of absorbers if each bound halo has a total cross section several times larger than πr_{vir}^2 . The inferred cross section depends on the fraction of observed OVI systems that are photoionized; if it is negligible, we find $\chi \approx 8$. If about half of the weak absorbers are photoionized (as suggested by some recent data; Prochaska et al. 2004), $\chi \approx 4$; however, this does not necessarily affect the predicted abundance of strong absorbers, which mostly arise from virial shocks. In our picture, the temperature of the infall shock increases with the central object’s mass (Furlanetto & Loeb 2004). Comparison to numerical simulations shows that these shocks are complex, with dense clumps of metal-enriched shocked gas embedded in a tenuous weakly-absorbing medium. They do confirm our key assumption, the association of hotter shocks with more massive systems (albeit with substantial scatter). In the future, we hope that more detailed comparisons to simulations will test other elements of our picture.

One of our most interesting results is that, while OVII and OVI can be associated with the same shocked system (even neglecting multiphase media from thermal instabilities), they do not

necessarily sample the same physical volume. As the gas flows away from the shock, it cools over a range of temperatures. OVII is presumably associated with gas closer to the shock, while OVI probes more distant gas. This calls into question modeling of the absorbers with single-temperature CIE gas. Figure 2 shows that gas with a more or less constant N_{OVII} can correspond to a wide range of N_{OVI} because of the range of temperatures through which the gas element cools, even if it remains near equilibrium at any single temperature (which may not be a valid assumption; Dopita & Sutherland 1996). The crucial point is that gas with $\Delta \sim 10\text{--}100$ and $T \sim 10^5\text{--}10^7 \text{ K}$ has a cooling time comparable to (though often a few times larger than) the Hubble time, so the temperature varies across the system.

The association of oxygen absorbers with virialization and infall shocks obviously implies that these systems must be spatially correlated with galaxy groups and clusters. This is not unique to our picture; any model that associates absorbers with large-scale shocks in the cosmic web must show a similar correlation. There appears to be a relatively strong correlation between OVI absorbers and galaxy groups: most lines of sight show galaxy overdensities coincident with the absorber locations (Tripp & Savage 2000; Savage et al. 2002; Richter et al. 2004), although it has not been statistically quantified and the correspondence is by no means perfect. Typical separations are $\lesssim 1 \text{ Mpc}$, suggesting that the correlation must extend significantly beyond the virial radius. Perhaps the clearest example lies along the line of sight toward PKS 2155–304, which has a pair of intergalactic OVI absorbers (Shull et al. 2003) offset by $\pm 400 \text{ km s}^{-1}$ from a galaxy group. Using *Chandra*, Fang et al. (2002) also found an OVIII absorber coincident with the galaxy group, although subsequent observations with *XMM* failed to confirm this detection. Because the line of sight passes near the barycenter of the group, the OVIII could correspond to virialized gas while the OVI systems probe gas that has not yet reached the virial radius but has nevertheless been shocked during infall. This is somewhat similar to the interpretation of Shull et al. (2003), who argued that the OVI and OVIII could trace multiphase infalling gas, although in their case they placed the gas in a single shocked region. However, we note that the OVII absorbers discovered by Nicastro et al. (2005) appear to show no correlation with galaxy systems. A more detailed study of the relation between galaxies and the known absorbers should shed light on the physical origin and significance of these systems. For example, photoionized OVI absorbers need not correlate with galaxies because they are not part of the filamentary structure.

Our model may also apply to the Local Group absorber. Nicastro et al. (2002) noted that all three ionization states appear along the line of sight to PKS 2155–304 with $N_{\text{OVI}} \sim 10^{14} \text{ cm}^{-2}$, $N_{\text{OVII}} \sim 4 \times 10^{15} \text{ cm}^{-2}$, and $N_{\text{OVIII}} \sim 5 \times 10^{15} \text{ cm}^{-2}$. They modeled the absorber as a single phase and favored a model with low-density photoionized gas. The comparable abundance of OVIII and OVII contrasted with the relatively large OVI column ruled out CIE. As a result the absorber was forced to have a physical size $\sim 5 \text{ Mpc}$. In our picture, the transitions sample different spatial locations and shocks. We can easily accommodate $N_{\text{OVII}}/N_{\text{OVI}}$ at infall shocks associated with halo masses $M \sim 10^{13} M_{\odot}$. The column density N_{OVIII} would be too small in such a shock; however, our privileged position near the center of the Milky Way and Local Group implies that this transition could be sampling a second, nearby shocked component at $T_{\text{vir}} \sim 2 \times 10^6 \text{ K}$. Thus the X-ray absorbers could be cosmological but no more than a few hundred kpc in extent. This is reassuring because, if every dark-matter halo comparable to the Local Group had a 5 Mpc hot gaseous halo, we

would expect to find several times as many high column-density OVII and OVIII absorbers as we see or as appear in simulations (Fang et al. 2002). In that case, the PKS 2155-304 line of sight would have to be unusual; however, comparable absorption columns appear along many other lines of sight through the Local Group (Rasmussen et al. 2003).

Our simple model is clearly not sophisticated enough for detailed predictions of the absorber statistics. For those purposes, cosmological simulations are much more appropriate (Cen et al. 2001; Fang & Bryan 2001; Fang et al. 2002). Chen et al. (2003) have presented the most detailed treatment to date. They showed that modern simulations do reproduce the observed number densities, at least to the (admittedly limited) accuracy of the current measurements and given an *ad hoc* (though reasonable) metallicity distribution. We have taken a complementary approach using analytic arguments to estimate the typical column densities and to parameterize the number densities in terms of the known abundance of collapsed objects. We believe that a combination of the two approaches should yield a much deeper physical understanding of the substantial baryon reservoir probed by these observations.

We are grateful to R. Cen and J. P. Ostriker for the use of their simulation results in Section 4 and to C. Danforth and J. M. Shull for sharing the data used in Fig. 6. We thank T. Fang and R. Davé for helpful conversations, A. Kravtsov for enlightening discussions, and M. Sako for clarifying issues associated with some of the early reports of IGM X-ray-absorption detections. SRF thanks the Kavli Institute for Theoretical Physics, where part of this work was completed under NSF PHY99-07949. This work was supported at Caltech in part by NASA NAG5-11985 and DoE DE-FG03-92-ER40701.

REFERENCES

Barkana R., Loeb A., 2001, Physics Reports, 349, 125

Bertschinger E., 1985, ApJS, 58, 39

Birnboim Y., Dekel A., 2003, MNRAS, 345, 349

Bryan G. L., Norman M. L., 1998, ApJ, 495, 80

Cen R., Ostriker J., 1992a, ApJ, 393, 22

Cen R., Ostriker J. P., 1992b, ApJL, 399, L113

Cen R., Ostriker J. P., 1999, ApJ, 514, 1

Cen R., Ostriker J. P., 2000, ApJ, 538, 83

Cen R., Tripp T. M., Ostriker J. P., Jenkins E. B., 2001, ApJL, 559, L5

Chen X., Weinberg D. H., Katz N., Davé R., 2003, ApJ, 594, 42

Croft R. A. C., et al., 2001, ApJ, 557, 67

Danforth C. W., Shull J. M., 2005, ApJ, submitted (astro-ph/0501054)

Davé R., et al., 2001, ApJ, 552, 473

Davé R., Tripp T. M., 2001, ApJ, 553, 528

Dopita M. A., Sutherland R. S., 1996, ApJS, 102, 161

Eisenstein D. J., Hu W., 1998, ApJ, 496, 605

Fang T., Bryan G. L., 2001, ApJL, 561, L31

Fang T., Bryan G. L., Canizares C. R., 2002, ApJ, 564, 604

Fang T., Marshall H. L., Lee J. C., Davis D. S., Canizares C. R., 2002, ApJL, 572, L127

Fang T., Sembach K. R., Canizares C. R., 2003, ApJL, 586, L49

Ferland G. J., 2001, Hazy, A Brief Introduction to Cloudy 94.00. <http://www.nublado.org/>

Furlanetto S. R., Loeb A., 2004, ApJ, 611, 642

Haardt F., Madau P., 1996, ApJ, 461, 20

Haardt F., Madau P., 2001, in Clusters of Galaxies and the High Redshift Universe Observed in X-rays, ed. D. M. Neumann & J. T. T. Van (21st Moriond Astrophysics Meeting, Les Arc, France) Modelling the UV/X-ray cosmic background with CUBA

Heckman T. M., Norman C. A., Strickland D. K., Sembach K. R., 2002, ApJ, 577, 691

Hellsten U., Gnedin N. Y., Miralda-Escudé J., 1998, ApJ, 509, 56

Hernquist L., 1990, ApJ, 356, 359

Jones C., Forman W., 1999, ApJ, 511, 65

Keres D., Katz N., Weinberg D. H., Davé R., 2004, MNRAS, submitted, (astro-ph/0407095)

Keshet U., Waxman E., Loeb A., Springel V., Hernquist L., 2003, ApJ, 585, 128

Nagai D., Kravtsov A. V., 2003, ApJ, 587, 514

Nagamine K., Cen R., Ostriker J. P., 2000, ApJ, 541, 25

Nagamine K., Fukugita M., Cen R., Ostriker J. P., 2001, ApJ, 558, 497

Nath B. B., Silk J., 2001, MNRAS, 327, L5

Navarro J. F., Frenk C. S., White S. D. M., 1997, ApJ, 490, 493

Nicastro F., et al., 2002, ApJ, 573, 157

Nicastro F., et al., 2005, Nature, in press (astro-ph/0412378)

Oegerle W. R., et al., 2000, ApJL, 538, L23

Pen U., 1999, ApJL, 510, L1

Perna R., Loeb A., 1998, ApJL, 503, L135

Prochaska J. X., et al., 2004, ApJ, in press, (astro-ph/0408294)

Rasmussen A., Kahn S. M., Paerels F., 2003, in ASSL Vol. 281: The IGM/Galaxy Connection. The Distribution of Baryons at $z=0$ X-ray IGM in the Local Group. p. 109

Rauch M., 1998, ARAA, 36, 267

Richter P., Savage B. D., Tripp T. M., Sembach K. R., 2004, ApJS, 153, 165

Rines K., Geller M. J., Kurtz M. J., Diaferio A., 2003, AJ, 126, 2152

Savage B. D., Sembach K. R., Tripp T. M., Richter P., 2002, ApJ, 564, 631

Sembach K. R., Howk J. C., Savage B. D., Shull J. M., Oegerle W. R., 2001, ApJ, 561, 573

Sheth R. K., Tormen G., 1999, MNRAS, 308, 119

Shull J. M., Tumlinson J., Giroux M. L., 2003, ApJL, 594, L107

Spergel D. N., et al., 2003, ApJS, 148, 175

Spitzer L., 1978, Physical Processes in the Interstellar Medium (New York: Wiley)

Sutherland R. S., Dopita M. A., 1993, ApJS, 88, 253

Tripp T. M., Savage B. D., 2000, ApJ, 542, 42

Tripp T. M., Savage B. D., Jenkins E. B., 2000, ApJL, 534, L1

Tumlinson J., Shull J. M., Giroux M. L., Stocke J. T., 2005, ApJ, in press (astro-ph/0411277)

Valageas P., Schaeffer R., Silk J., 2002, A&A, 388, 741

Wang L., Caldwell R. R., Ostriker J. P., Steinhardt P. J., 2000, ApJ, 530, 17

White S. D. M., Frenk C. S., 1991, ApJ, 379, 52

Wu K. K. S., Fabian A. C., Nulsen P. E. J., 2001, MNRAS, 324, 95

Xue Y., Wu X., 2003, ApJ, 584, 34